

Article

A Study on the Skin Adhesion Test of Fine Particles by Brake Pad Friction

Jae Sang Yoo * and Young Ze Lee *

Mechanical Engineering, SungKyunKwan University, Seoul 16419, Republic of Korea

* Correspondence: yjszzangoh@skku.edu (J.S.Y.); yzlee@skku.edu (Y.Z.L.); Tel.: +82-10-2988-0226 (Y.Z.L.)

Abstract: Though fine dust on the side of the road has decreased substantially due to environmental regulations, the adverse effects on the human due to air pollution still cannot be ignored. In this study, we aim to determine the effect of the vehicle's brake usage on air pollution and the human skin according to the brake pad conditions. A friction experiment device simulating the mechanical friction of a vehicle brake pad was designed to conduct a fine particle generation experiment. Different loads and rpms were set under the friction and the fine particles generated through this were analyzed using an ELPI+ (Electrical Low Pressure Impactor) apparatus. At the same time as the friction experiment was conducted, a human skin sample was installed around it, and after the experiment, the deposited fine dust was observed under a microscope for each certain area. The experiment found that there was a change in micrometer-sized microparticles affecting PM (Particulate Matter) depending on the brake pad conditions. In addition, a result graph of the adhesion of fine particles according to skin surface conditions and brake pad conditions was derived. A discussion was performed on how the fine particles affect the human skin through the characteristics of the fine particles according to the friction conditions.

Keywords: airborne particles; brake pad; friction; pollution



Citation: Yoo, J.S.; Lee, Y.Z. A Study on the Skin Adhesion Test of Fine Particles by Brake Pad Friction. *Lubricants* **2022**, *10*, 338. <https://doi.org/10.3390/lubricants10120338>

Received: 1 November 2022

Accepted: 26 November 2022

Published: 29 November 2022

Publisher's Note: MDPI stays neutral with regard to jurisdictional claims in published maps and institutional affiliations.



Copyright: © 2022 by the authors. Licensee MDPI, Basel, Switzerland. This article is an open access article distributed under the terms and conditions of the Creative Commons Attribution (CC BY) license (<https://creativecommons.org/licenses/by/4.0/>).

1. Introduction

Particulate air pollution originates from anthropogenic natural sources. Traffic intensity is an important determinant of ambient anthropogenic PM concentrations, but its contribution differs with the size of PM. It is known that the PM10 consists of crustal matter, organic compounds, hydrocarbons, and bacteria, and that it is produced by mechanical processes rather than combustion. On the other hand, PM2.5 is mainly produced by the combustion process with secondary particles made by chemical reactions with metals, hydrocarbons, and atmospheric gas compounds [1]. Recent studies show that non-exhaust particle emissions have come to frequently exceed exhaust emissions, which remains one of the primary sources of particulate matter (PM) in the atmosphere in urban areas. These non-exhaust particles include brake, tire, road surface abrasion, and resuspension in the wake of passing traffic. Due to the complex environment and conditions, it is not easy to quantify the emissions in both laboratory and field conditions [2,3]. In this study, the friction of the brake pad was tested, and it was found to contribute greatly to the non-exhaust particle emission.

Studies have shown that PM has harmful effects on the human body, not only on the respiratory system but also on the skin. The skin barrier is an important protective barrier that regulates the external penetration of water, nutrients, ions, and environmental stimuli, as well as internal and external penetration. PM exposure can disrupt skin barrier functions through oxidative stress and pro-inflammatory cytokines [4–6]. The polycyclic aromatic hydrocarbons (PAHs) that are adsorbed on the PM surface can cause health hazards due to their ability to induce the formation of reactive oxygen species (ROS) [7]. PM exposure can further disrupt the skin barrier with a pre-existing barrier dysfunction [8]. Epidemiological

studies have provided sufficient evidence of a positive association between PM exposure and the induction of adverse health effects [1]. The effect of microparticles penetrating into human skin depends on the size and type of formulation to which the microparticles are topically applied. Fine particles with a diameter of 1 micrometer or more hardly penetrate human skin. They are located on the surface of the skin and form a film that can be used for purposes such as protection against ultraviolet (UV) radiation in sunscreens [9]. TiO₂ in sunscreens penetrates the human stratum corneum (SC) and can be visualized in some hair follicles, including deeper areas. However, their presence cannot be interpreted as penetration into the living layers of the skin, because this part of the hair follicle channel is also covered by the SC barrier. As a result, the penetration of TiO₂ particles into living tissues cannot be observed, even with a very sensitive method [10]. However, if PM enters the skin where the barrier is broken, it can cause inflammation and have a detrimental effect on the skin [6].

In conducting skin-related research, there is a method using artificial skin (vitro) and a method using real skin (vivo). Vitro models which include normal human dermal fibroblasts (NHDF), human skin equivalent (HSE), human epidermis equivalent (HEE) resemble many characteristics of native human skin but have a limitation of morphogenesis and barrier formation. The difference between in vitro and in vivo skin may have been caused by suboptimal cell culture conditions in which the oxygen levels in vitro were much higher than those in vivo. Most of the current in vitro models lack information on the inflammatory system, vasculature, and other properties of the underlying skin, thereby necessitating a range of physiologically more complex models [11–13]. Representative vivo research methods include methods using human and animal skins. In the case of PM penetration work, rodent skin differs from human skin, as its significantly thinner skin layer and higher hair follicle density lead to higher material penetration. Conversely, pig skin more closely resembles the structural properties of human skin [14,15]. An animal model is used to compare the effects of PM on skin with healthy and disrupted barrier function. A disrupted barrier can be created by conventional tape stripping methods, which basically involve the layer-by-layer removal of SC from animal skin models. This model has been used to study different aspects of inflammatory skin diseases and investigate the penetration of compounds through the skin [16–18]. However, animal models have the disadvantages of different physiological structures, being inefficient in terms of time and money, and being limited by many regulations and numerous ethical issues. For these reasons, alternatives to animal testing, such as 2D or 3D vitro human skin models, should be considered [19].

In skin experiments, it is necessary to distinguish the compartments of the skin barrier, which is composed of physical, microbial, chemical, and immunological barriers. Most of the studies on PM penetration have investigated the effect on physical barriers, and in fact, PM penetration does not often affect other barriers due to the different epidermal layers of the main cells, molecules, or micro-organisms which contribute to each barrier function [20]. Despite the lack of studies on chemical and microbial barriers, some studies have shown that PM exposure has an adverse effect on skin barrier. Regarding the effect of PM_{2.5} exposure on the cholesterol metabolism, it was found that there was a final increase of cholesterol and decrease of squalene [21]. The antimicrobial peptides, serving as a chemical barrier compartment, were observed to increase in 3D human epidermal equivalent treated with PM [22]. Several natural extracts have been found to have a positive effect on chemical barriers. Green tea extract (GTE) effectively inhibits the damage induced by PM_{2.5}, including reversing PM_{2.5}-stimulated cholesterol synthesis, and Camellia japonica flower extract (CJFE) has protective effects against the mechanism of skin aging activated by urban air pollutants [21,23].

Considering the importance of the human health and the seriousness of the effect of PM on human skin, an experimental study has been conducted and reported in this article. We concluded that PM's skin adhesion experiment does not matter whether it is vivo or vitro, and we decided to use a sample of vivo skin. In addition, in the case of this experiment, the

effect on the skin barrier is seemed to be negligible because penetration is assumed further after the PM adhesion on the skin surface. Additional detailed experimental settings are described in the following sections

2. Materials and Methods

To express PM caused by the brake of the vehicle, a specimen unit of the experimental equipment was constructed to simulate friction between the brake pad and the rotor of the vehicle. Regarding the friction type, a pin-on-disk model capable of applying constant pressure to the rotating disk was selected. NAO (Non-Asbestos Organic) brake pad was manufactured to disc specimen and fixed to the rotating shaft. Precise elemental compositions of the brake pad are listed in Table 1. Grey cast iron was cut into a pin type specimen and grabbed firmly above the disc specimen. The size of specimen was $10 \times 5 \times 10$ mm (width \times depth \times height) and the surface of the friction was curved for the constant pressure.

Table 1. Elemental compositions of the brake pad material, wt.%.

Element	Brake Pad Specimen
Ba	31.1
Fe	15.56 ¹
Ca	7.2
S	5.08
Al	3.52
Si	3.42
K	1.37
Zn	1.31
Sr	0.419
Mg	0.36
Mn	0.12

The experiment was conducted under the conditions of loads and rpms. Loads of 5 kg and 10 kg were applied with the rotating motor conditions of 180 and 360 rpm. The operation was carried out for a short period of time (30 min) considering the chemical degeneration of brake pads caused by high temperatures. All tests were conducted at room temperature, and repeated tests were performed five times to ensure the precision of the experiment. Table 2 shows the conditions used in the specimen test, as well as the setting of the vehicle assumed in the experiment. The brake pad is cut in half to fit the lower specimen zig, which is located above the disc. A schematic view of the experiment is shown in Figure 1. The conditions should match the real vehicle brake system, and to achieve this, there should be standards of conditions. A theoretical equation was used to calculate the energy of the real vehicle brake system, while simultaneously calculating the one with the brake pad wear test [24]. It is difficult to simulate the friction of the brake pad of an actual vehicle with specimen equipment. To solve this problem, the method of calculating the heat energy applied per unit area of the actual pad was selected. The thermal energy generated when a passenger car with arbitrary conditions was applied in the brake was calculated according to the following process.

Table 2. Values and units of the main factor and the conditions of specimen test.

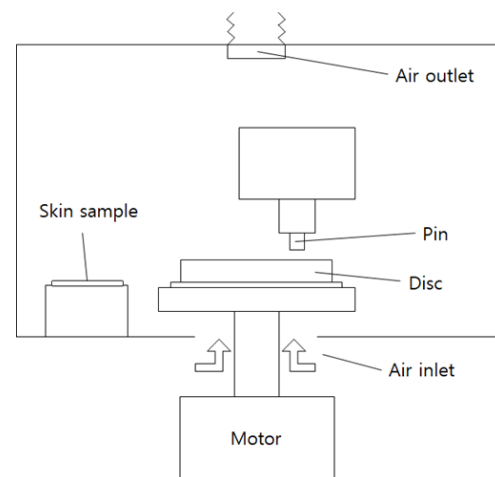
	Values	Units
Vehicle mass (m)	1600	kg
Correction factor for rotating masses (k)	1	-
Heat distribution on rotor	0.9	-

Table 2. Cont.

	Values	Units
Tire slip (s)	0.08	-
Swept area of 1 brake side	67	cm ²
Initial brake temperature	300	K
Speed of vehicle	60	km/h
Deceleration (a)	0.75, 1, 1.5, 2, 2.5	m/s ²
Test load	5, 10	kg
Test rpm	180, 360	-
Temperature	298–300	K



(a)



(b)

Figure 1. (a) Actual view of experimental equipment. (b) Schematic view of the friction experiment.

When the vehicle decelerates to a higher velocity V_1 to V_2 , the braking energy E_b is

$$E_b = \left(\frac{m}{2}\right)(V_1^2 - V_2^2) + \left(\frac{I}{2}\right)(\omega_1^2 - \omega_2^2), \text{ Nm(lbft)} \quad (1)$$

where I = mass moment of inertia of rotating parts, $\text{kgm}^2(\text{lbft}^2)$.

m = vehicle mass, $\text{kg}(\text{lbs}^2/\text{ft})$

V_1 = velocity at begin of braking, $\text{m/s}(\text{ft/s})$

V_2 = velocity at end of braking, $\text{m/s}(\text{ft/s})$

ω_1 = angular velocity of rotating parts at beginning of braking, $(1/\text{s})$

ω_2 = angular velocity of rotating parts at end of braking, $(1/\text{s})$

If the vehicle comes to a complete stop, $V_2 = \omega_2 = 0$, and Equation (1) become

$$E_b = \frac{mV_1^2}{2} + \frac{I\omega_1^2}{2}, \text{ Nm(lbft)} \quad (2)$$

When all rotating parts are expressed relative to the revolutions of the wheel, then with $V = R\omega$, Equation (2) becomes

$$E_b = \frac{m}{2} \left(1 + \frac{I}{R^2m}\right) V_1^2 \approx \frac{kmV_1^2}{2}, \text{ Nm(lbft)} \quad (3)$$

where k = correction factor for rotating masses ($k \approx 1 + I/R^2m$)
 R = tire radius, m(ft)

Typical values of k for passenger cars range from 1.05 to 1.15 in high gear to 1.3 to 1.5 in low gear. The corresponding values for trucks are 1.03 to 1.06 and 1.25 to 1.6, respectively. Braking power P_b is equal to braking energy divided by the time t during which braking occurs.

$$P_b = d(E_b)/dt, \text{ Nm/s(lbft/s)} \quad (4)$$

If the deceleration a is constant, then the velocity $V(t)$ is given by

$$V(t) = V_1 - at, \text{ m/s(ft/s)} \quad (5)$$

where a = deceleration, m/s^2 (ft/s^2)

t = time, s

Equations (3) through (5) yield the brake power as

$$P_b = kma(V_1 - at), \text{ Nm/s(lbft/s)} \quad (6)$$

Close inspection of Equation (6) reveals that braking power does not stay constant during the braking process. At the beginning of braking ($t = 0$), brake power is at a maximum, and it decreases to zero when the vehicle stops. The time t_s for the vehicle to come to a stop is

$$t_s = V_1/a, \text{ second} \quad (7)$$

The average braking power P_b over the braking time t_s for a vehicle coming to stop is

$$P_b = kmaV_1/2, \text{ Nm/s(lbft/s)} \quad (8)$$

Equation (8) shows the basic, general calculations of the energy absorption. The tire slip, heat distribution, brake area, and percentage braking on brake pad should all be considered. Tire slip is defined by the ratio of the difference between vehicle forward speed and circumferential speed to vehicle forward speed. Table 2 lists the values and units of the main factor used to calculate the energy absorption.

For research, a frozen full thickness skin sheet of healthy humans was used. Skins were stored frozen and thawed whenever necessary for experiments. During experiments, skins were installed inside the chamber with small holes (10 mm diameter) exposed to the air. Several conditions were selected in consideration of the skin surface condition (normal, rubbing, sunscreen, lotion). In the case of sunscreen, products containing titanium oxide were selected without any special additives. For lotion, 'all skin type' products containing moisturizer ingredients without special additives were selected. In the case of rubbing, it was assumed that external pressure was applied to the skin. A sterilized stick was rubbed on the skin surface five times with constant force. In the case of additives, a small amount was applied to the skin, spread with a sterilized stick, and left for 30 min. See the Table 3 for detailed setting and conditions.

Table 3. Details about the skin surface conditions for cases 1–4.

Case	Setting	Condition
1	Normal skin	-
2	Normal skin with rubbing	0.5 N, 5 times
3	Normal skin + sunscreen	1 mg/cm ²
4	Normal skin + lotion	1 mg/cm ²

An experiment was conducted after confirming that the pattern of the skin could be distinguished by observing it under a microscope. After the experiment, each hole was divided into nine sectors, and the particles were observed and analyzed under a microscope. The ratio of PM10 to PM2.5 for each condition was investigated by synthesizing the size and

number of particles on the skin surface. For PM analysis, the experiment was conducted, and fine particles were analyzed using Electrical Low Pressure Impactor (ELPI) equipment at the same time.

3. Results

A microscopic survey was conducted according to the friction conditions, and a graph showing the average number of particles per area of 1 mm^2 according to each skin surface condition was derived. Cases 1–4 on the horizontal axis respectively represent normal skin, rubbed skin, sunscreen, and lotion. The skin surface seen through microscopic observation is shown in Figure 2. PM appeared as a black dot on the skin surface, and the average number was calculated by dividing PM10 and PM2.5 by the size of PMs in each area. Figure 3 shows the results with differing friction environment, and the error distribution according to the condition of each skin condition is calculated and graphically demonstrated. It shows that normal skin (case 1) and rubbed skin (case 2) were both observed as having a small number of particles on the surface, and the error was not significant, even after repeated experiments, except for in the 10 kg 360 rpm experiment. In the case of 5 kg experiments, an error occurs when additives are added to the surface of the skin, and when lotion is applied (case 4), it increases simultaneously with the total amount of PM. The addition of sunscreen (case 3) seems to not have much of an effect compared to normal skin (case 1). In 180 rpm, the number of particles in case 1–3 does not exceed the total of 10, whereas case 4 exceeds 40. Figure 4 has a graph, such as in Figure 3, but there is a difference in the total average number of particles. Overall, it shows an increase by about twice as much as PM. Similarly, the PM amount and error rate of case 4 are both quite high. The PM adhesion of normal skin rises abnormally when the load is increased to 10 kg. The number of particles of 5 kg 360 rpm remained similar even though the load was increased in cases 3 and 4.

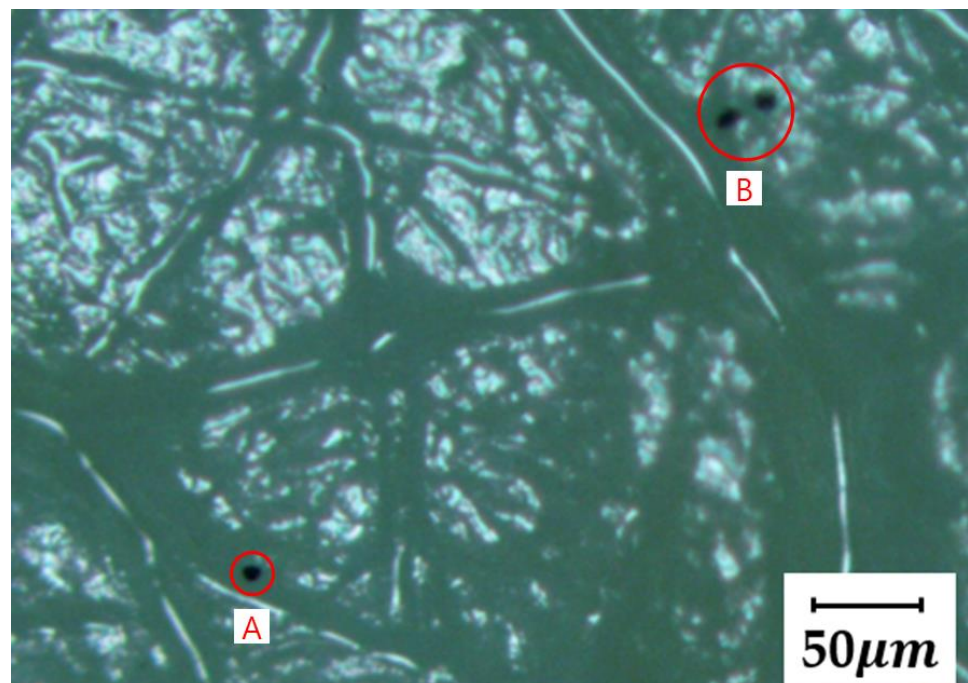
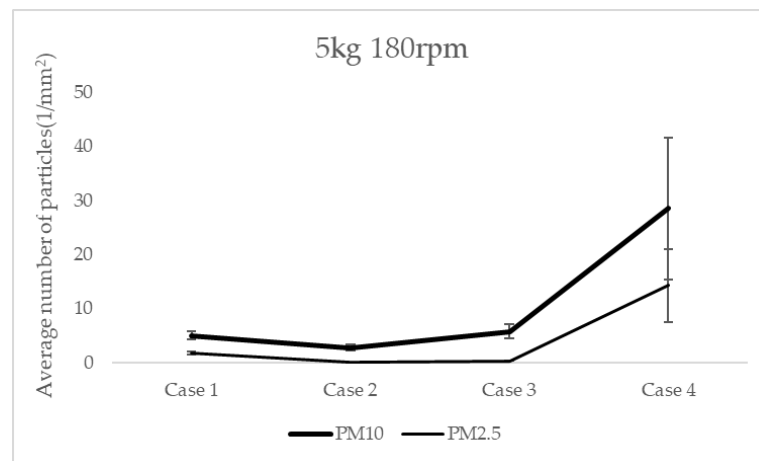
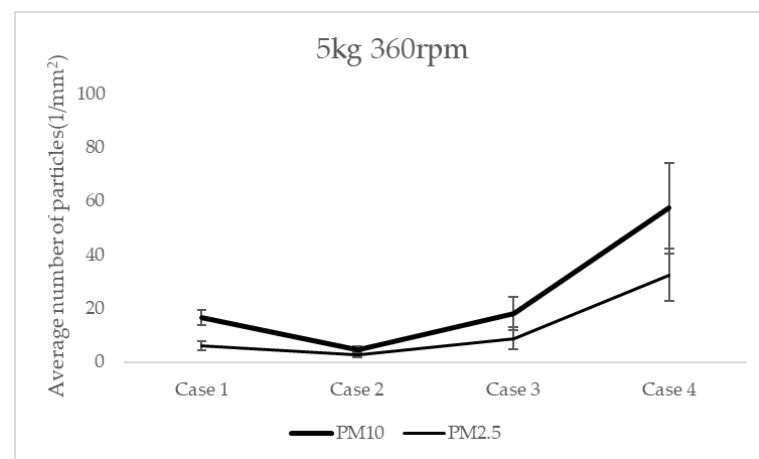


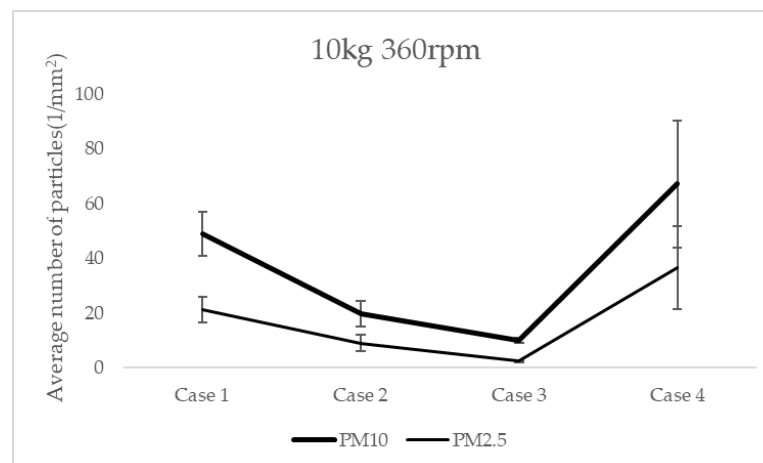
Figure 2. Observation of the skin surface, PM size, and number observed under a microscope (A). Depending on the skin penetration distance of the fine particles, the microscope may not focus and appear blurred (B).



(a)



(b)



(c)

Figure 3. (a) Average number of particles on human skin surface with cases 1–4 in the friction condition of 5 kg 180 rpm. (b) Average number of particles on human skin surface with cases 1–4 in the friction condition of 5 kg 360 rpm. (c) Average number of particles on human skin surface with cases 1–4 in the friction condition of 10 kg 360 rpm.

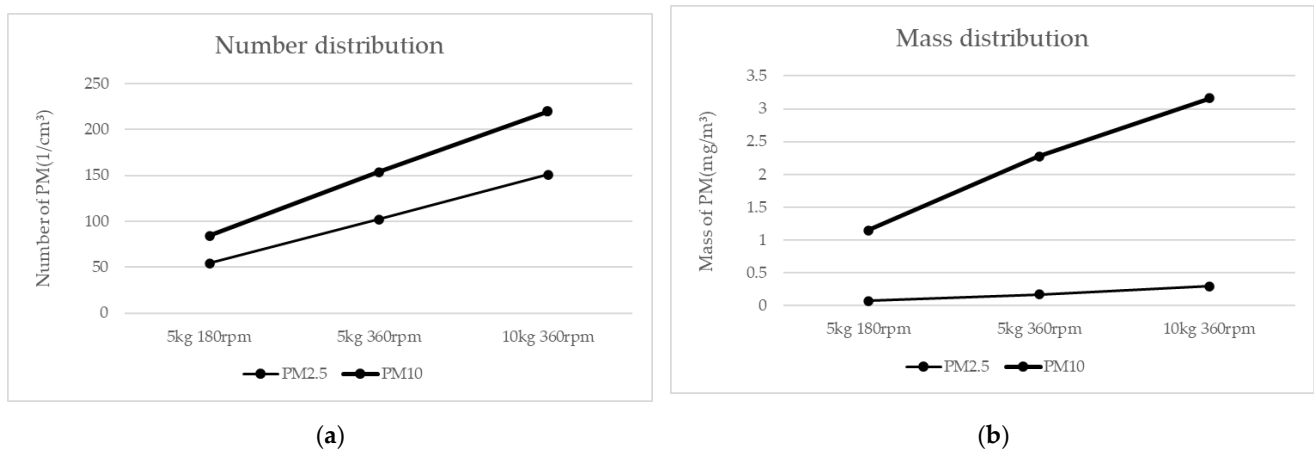


Figure 4. Average number distribution (a) and average mass distribution (b) of each case using ELPI apparatus.

Figure 4 shows the results of the analysis using ELPI equipment. It expresses the number and mass of PM per unit area according to each friction condition. The results were derived by extracting only microscopically identifiable parts of the data, excluding those for ultrafine particles with an average diameter of 0.8 μm or less. In the case of number distribution, the PM number of $1/\text{cm}^3$ was calculated, and for mass distribution, the PM mass of mg/m^3 was calculated. The results of each experiment are shown in a graph, indicating a linear shape, meaning that the number of fine particles generated can be controlled by the load and the rpm. PM2.5 shows a very sophisticated linearly proportional relationship (with the number of PMs being 54, 101, and 150, respectively). It is possible to calculate the probability of adhesion to the skin through the average PM distribution. The results for the average number of particles adhered to the skin of the unit area were found. By dividing the average number of particles floating in the air, the result for the tendency of average adhesion rate for the unit area can be obtained, which is described in Figure 5. Through these results, the increase in load causes an irregular effect on the generation of particles above PM2.5 and below PM10, which is also evident in the adhesion of the skin surface. In the case of the lotion additive in case 4, the oil component of the lotion seems to have affected the adhesion of fine particles, and the reason for the high variability of the error bar is also analyzed as this cause.

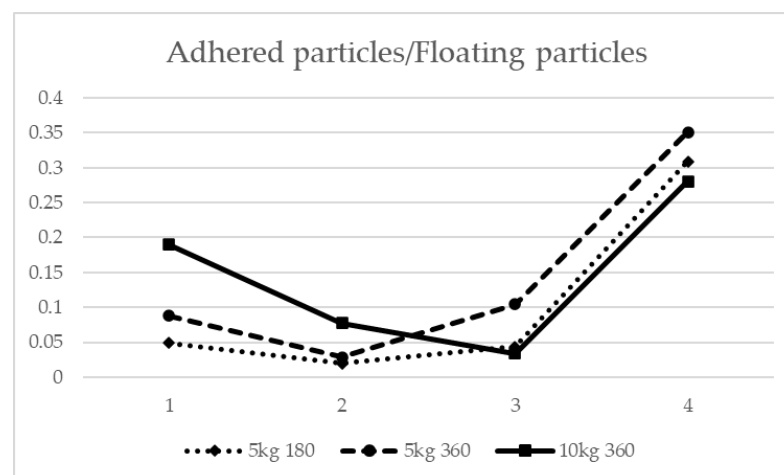


Figure 5. Tendency of adhesion rate on skin with the number distribution calculated. Average number of particles adhered to unit area of skin ($1/\text{mm}^2$) is divided by the average number of floating particles ($1/\text{cm}^3$).

4. Discussion

From Figure 5, there is a clear difference in the adhesion of fine particles according to the components of products. In case 3, the error is very small, and the experimental results are similar to those of case 1, while case 4 has a very large error and a high ratio of fine particle adhesion in all experiments. This is presumed to be caused by the concentration of additives on the inner dents of skin with the passage of time rather than covering all sides such as coatings on the skin surface. Therefore, the area exposed to air can be expressed in a continuous pattern shape of the additive and skin. This seems to serve to flatten the unevenness of the skin surface and reduce the adhesion caused by irregularities in the skin (case 3). However, since the oil component of the additive catches the fine particles, the amount of condensation increases (case 4). Case 2, which assumes rubbing of the skin, shows a significant decrease in the adhesion rate compared to normal skin, which means that the adhesion of fine particles on the skin surface can be solved with a little treatment. However, the report stated that small sunscreen particles such as fine particles can penetrate deep into the skin when additives such as sunscreen are applied to the skin and left unattended for a long time [10]. Although it does not cause serious skin inflammation due to the inability to penetrate the dermal layer of the skin, it is possible to stick inside the SC for a long time. Further, studies using damaged skin barrier samples confirmed that the penetration of PM increased reactive oxygen species (ROS) production and caused skin inflammation. ROS and skin inflammations end up with skin barrier disruption [6,25]. Particles can even enter the depths near the dermis of the skin through the hair follicles. The area near the hair follicle is also blocked by skin barriers, but if hair roots are removed by external pressure, there is a possibility that the remaining fine particles can directly penetrate the dermal layer. In contrast to the penetration of fine particles into the skin, which exhibits an immediate response, PM in the air does not have any notable changes on human skin. However, it is reported that repeated PM exposure to skin on a daily basis can have a negative impact, such as skin aging [4,26–28]. All skin age mechanisms indicated the induction of an inflammatory cascade and the resulting disruption of the skin barrier. Overall, fine particles floating in the air continue to adhere to the skin, causing skin aging, breaking skin barriers, and further showing the possibility of penetrating deeply into the skin. The fine particle components generated from the brake pads have been reported to be quite harmful. Brake pads are classified as physical friction, but they can also cause chemical denaturation due to harsh environments under high loads at high temperatures, thus resulting in many ultrafine particles [29,30]. Due to the difficulty associated with observing ultrafine particles, only PM10 and PM2.5 were considered in the study, but large amounts of ultrafine particle emission were confirmed using ELPI equipment. Reports stated that the characteristics of particles generated in the pad vary depending on the temperature during the brake pad friction process. This is also presumed to be due to chemical degradation, with a rapid increase in the emission of ultrafine particles in a specific high-temperature region [31]. In general, chemical changes in the brake pad are carried out at 300 °C, and in some papers, a large number of ultrafine particles have been detected around 160 °C and up to 200 °C [32,33]. However, there is not much need for consideration of extreme environments, as the braking system of vehicles generally does not exceed 200 °C [34]. Just as ultrafine particles have a harmful effect on the human respiratory system, they are expected to have a negative effect if they adhere to the skin surface and penetrate inside, with the disruption of the barrier.

5. Conclusions

The conclusions obtained through this study are as follows: 1. Through an experiment that simulates the friction of the actual brake pad, a large amount of PM is generated on the brake pad. The amount of PM generated is generally proportional to rpm and load, which is generally the same as the heat energy calculated. 2. As a result of checking the skin sample, some of the floating PMs were found to be deposited on the skin surface, which was mostly detached with a slight rub. Sunscreen additives had similar results to normal skin, but in

the case of lotion, skin adhesion differed by 1.5 to 3 times. 3. As a result of calculating the average number of suspended fine particles for the number of adhesion of fine particles to the skin unit area, the skin adhesion rate tended not to be affected by the load and rpm. This study set the load and rpm as the experimental conditions because the research was conducted at a low temperature at which the chemical change of the brake pad was not considered. Therefore, this study can be a data source for researchers conducting research on air pollution causes and its impact on human skin, since the environment considered in this work is the one with which ultrafine particles are generally detected upon a chemical change in brake pads.

Author Contributions: Conceptualization, J.S.Y. and Y.Z.L.; investigation, J.S.Y.; writing—original draft preparation, J.S.Y.; writing—review and editing, J.S.Y.; supervision, Y.Z.L. All authors have read and agreed to the published version of the manuscript.

Funding: This research received no external funding.

Data Availability Statement: Not applicable.

Conflicts of Interest: The authors declare no conflict of interest.

References

1. de Kok, T.M.C.M.; Driee, H.A.L.; Hogervorst, J.G.F.; Briedé, J.J. Toxicological assessment of ambient and traffic-related particulate matter: A review of recent studies. *Mutat. Res. Rev. Mutat. Res.* **2006**, *613*, 103–122. [[CrossRef](#)] [[PubMed](#)]
2. Penkała, M.; Ogrodnik, P.; Rogula-Kozłowska, W. Particulate Matter from the Road Surface Abrasion as a Problem of Non-Exhaust Emission Control. *Environments* **2018**, *5*, 9. [[CrossRef](#)]
3. Thorpe, A.; Harrison, R.M. Sources and properties of non-exhaust particulate matter from road traffic: A review. *Sci. Total Environ.* **2008**, *400*, 270–282. [[CrossRef](#)]
4. Mancebo, S.E.; Wang, S.Q. Recognizing the impact of ambient air pollution on skin health. *J. Eur. Acad. Dermatol. Venereol.* **2015**, *29*, 2326–2332. [[CrossRef](#)] [[PubMed](#)]
5. Kim, K.; Cho, D.; Park, H. Air pollution and skin diseases, Adverse effects of airborne particulate matter on various skin diseases. *Life Sci.* **2016**, *152*, 126–134. [[CrossRef](#)] [[PubMed](#)]
6. Jin, S.P.; Li, Z.; Choi, E.K.; Lee, S.; Kim, Y.K.; Seo, E.Y.; Chung, J.H.; Cho, S. Urban particulate matter in air pollution penetrates into the barrier-disrupted skin and produces ROS-dependent cutaneous inflammatory response in vivo. *J. Dermatol. Sci.* **2018**, *91*, 175–183. [[CrossRef](#)] [[PubMed](#)]
7. Tobiszewski, M.; Namieśnik, J. PAH diagnostic ratios for the identification of pollution emission sources. *Environ. Pollut.* **2012**, *162*, 110–119. [[CrossRef](#)]
8. Dijkhoff, I.M.; Drasler, B.; Karakocak, B.B.; Petri-Fink, A.; Valacchi, G.; Eeman, M.; Rothen-Rutishauser, B. Impact of airborne particulate matter on skin, a systematic review from epidemiology to in vitro studies. *Part. Fibre Toxicol.* **2020**, *17*, 35. [[CrossRef](#)] [[PubMed](#)]
9. Lademann, J.; Schaefer, H.; Otberg, N.; Teichmann, A.; Blume-Peytavi, U.; Sterry, W. Penetration of microparticles into human skin. *Life Sci.* **2004**, *55*, 1117–1119.
10. Lademann, J.; Weigmann, H.-J.; Rickmeyer, C.; Barthelmes, H.; Schaefer, H.; Mueller, G.; Sterry, W. Penetration of Titanium Dioxide Microparticles in a Sunscreen Formulation into the Horny Layer and the Follicular Orifice. *Skin Pharmacol. Appl. Skin Physiol.* **1999**, *12*, 247–256. [[CrossRef](#)] [[PubMed](#)]
11. Mieremet, A.; Rietveld, M.; Absalah, S.; van Smeden, J.; Bouwstra, J.A.; El Ghalbzouri, A. Improved epidermal barrier formation in human skin models by chitosan modulated dermal matrices. *PLoS ONE* **2017**, *12*, e0174478. [[CrossRef](#)] [[PubMed](#)]
12. Mieremet, A.; Vázquez García, A.; Boiten, W.; van Dijk, R.; Gooris, G.; Bouwstra, J.A.; El Ghalbzouri, A. Human skin equivalents cultured under hypoxia display enhanced epidermal morphogenesis and lipid barrier formation. *Sci. Rep.* **2019**, *9*, 7811. [[CrossRef](#)]
13. Pupovac, A.; Senturk, B.; Griffoni, C.; Maniura-Weber, K.; Rottmar, M.; McArthur, S.L. Toward Immunocompetent 3D Skin Models. *Adv. Heal. Mater.* **2018**, *7*, e1701405. [[CrossRef](#)] [[PubMed](#)]
14. Todo, H. Transdermal Permeation of Drugs in Various Animal Species. *Pharmaceutics* **2017**, *9*, 33. [[CrossRef](#)] [[PubMed](#)]
15. Debeer, S.; LE Ludec, J.-B.; Kaiserlian, D.; Laurent, P.; Nicolas, J.F.; Dubois, B.; Kaniakakis, J. Comparative histology and immunohistochemistry of porcine versus human skin. *Eur. J. Dermatol.* **2013**, *23*, 456–466. [[CrossRef](#)]
16. Berkers, T.; Boiten, W.A.; Absalah, S.; van Smeden, J.; Lavrijsen, A.P.M.; Bouwstra, J.A. Compromising human skin in vivo and ex vivo to study skin barrier repair. *Biochim. Biophys. Acta. Mol. Cell Biol. Lipids* **2019**, *1864*, 1103–1108. [[CrossRef](#)]
17. Gerritsen, M.J.P.; van Erp, P.E.J.; van Vlijmen-Willems, I.M.J.J.; Lenders, L.T.M.; van de Kerkhof, P.C.M. Repeated tape stripping of normal skin: A histological assessment and comparison with events seen in psoriasis. *Arch. Dermatol. Res.* **1994**, *286*, 455–461. [[CrossRef](#)] [[PubMed](#)]

18. Gao, Y.; Wang, X.; Chen, S.; Li, S.; Liu, X. Acute skin barrier disruption with repeated tape stripping: An in vivo model for damage skin barrier. *Skin Res. Technol.* **2013**, *19*, 162–168. [[CrossRef](#)] [[PubMed](#)]
19. Rollin, B.E. Toxicology and New Social Ethics for Animals. *Toxicol. Pathol.* **2003**, *31*, 128–131. [[CrossRef](#)] [[PubMed](#)]
20. Niehues, H.; Bouwstra, J.A.; El Ghalbzouri, A.; Brandner, J.M.; Zeeuwen, P.L.; van den Bogaard, E.H. 3D skin models for 3R research: The potential of 3D reconstructed skin models to study skin barrier function. *Exp. Dermatol.* **2018**, *27*, 501–511. [[CrossRef](#)]
21. Liao, Z.; Nie, J.; Sun, P. The impact of particulate matter (PM_{2.5}) on skin barrier revealed by transcriptome analysis focusing on cholesterol metabolism. *Toxicol. Rep.* **2020**, *7*, 1–9. [[PubMed](#)]
22. Kim, H.-J.; Bae, I.-H.; Son, E.D.; Park, J.; Cha, N.; Na, H.-W.; Jung, C.; Go, Y.-S.; Kim, D.-Y.; Lee, T.R.; et al. Transcriptome analysis of airborne PM_{2.5}-induced detrimental effects on human keratinocytes. *Toxicol. Lett.* **2017**, *273*, 26–35. [[CrossRef](#)] [[PubMed](#)]
23. Kim, M.; Son, D.; Shin, S.; Park, D.; Byun, S.; Jung, E. Protective effects of Camellia japonica flower extract against urban air pollutants. *BMC Complement. Altern. Med.* **2019**, *19*, 30. [[CrossRef](#)]
24. Rudolf, L. *Brake Design and Safety*; Society of Automotive Engineers: Warrendale, PA, USA, 1999.
25. Zheng, R.; Tao, L.; Jian, H.; Chang, Y.; Cheng, Y.; Feng, Y.; Zhang, H. NLRP3 inflammasome activation and lung fibrosis caused by airborne fine particulate matter. *Ecotoxicol. Environ. Saf.* **2018**, *163*, 612–619. [[CrossRef](#)]
26. Krutmann, J.; Liu, W.; Li, L.; Pan, X.; Crawford, M.; Sore, G.; Seite, S. Pollution and skin: From epidemiological and mechanistic studies to clinical implications. *J. Dermatol. Sci.* **2014**, *76*, 163–168. [[CrossRef](#)] [[PubMed](#)]
27. Peng, F.; Xue, C.-H.; Hwang, S.K.; Li, W.-H.; Chen, Z.; Zhang, J.-Z. Exposure to fine particulate matter associated with senile lentigo in Chinese women a cross-sectional study. *J. Eur. Acad. Dermatol. Venereol.* **2017**, *31*, 355–360. [[CrossRef](#)] [[PubMed](#)]
28. Burke, K.E. Mechanisms of aging and development—A new understanding of environmental damage to the skin and prevention with topical antioxidants. *Mech. Ageing Dev.* **2017**, *172*, 123–130. [[CrossRef](#)] [[PubMed](#)]
29. Alemani, M.; Nosko, O.; Metinoz, I.; Olofsson, U. A Study on Emission of Airborne Wear Particles from Car Brake Friction Pairs. *Int. J. Mater. Manuf.* **2015**, *9*, 147–157. [[CrossRef](#)]
30. Uexküll, O.; Skerfving, S.; Doyle, R.; Braungart, M. Antimony in brake pads—a carcinogenic component? *J. Clean. Prod.* **2005**, *13*, 19–31. [[CrossRef](#)]
31. Wahlström, J.; Söderberg, A.; Olander, L.; Jansson, A.; Olofsson, U. A pin-on-disc simulation of airborne wear particles from disc brakes. *Wear* **2010**, *268*, 763–769. [[CrossRef](#)]
32. Nosko, O.; Olofsson, U. Quantification of ultrafine airborne particulate matter generated by the wear of car brake materials. *Wear* **2017**, *374–375*, 92–96. [[CrossRef](#)]
33. Nosko, O.; Vanhanen, J.; Olofsson, U. Emission of 1.3–10 nm airborne particles from brake materials. *J. Aerosol Sci.* **2017**, *51*, 91–96. [[CrossRef](#)]
34. Garg, B.D.; Cadle, S.H.; Mulawa, P.A.; Groblicki, P.J. Brake wear particulate matter emissions. *Environ. Sci. Technol.* **2000**, *34*, 4463–4469. [[CrossRef](#)]